Continuous conveying and mixing characteristics of high viscosity materials under acoustic vibration excitation

Xiaobin Zhan[a*], Binhuan Ye[a], Biran Li[a] and Tielin Shi[a]

[a]State Key Lab of Digital Manufacturing Equipment and Technology, Huazhong University of Science and Technology, Wuhan 430074, China

[*]Email address for correspondence: zhanxb@hust.edu.cn

Abstract

Investigating the conveying and mixing characteristics of high-viscosity fluids in an inclined flow channel under the excitation of acoustic frequency vibrations using computational fluid dynamics (CFD) methods. As the intensity of the acoustic vibration excitation increases, the free surface of the liquid transitions from generating Faraday waves to generating disordered jets. Continued increase in the amplitude leads to the liquid filling most of the vessel space, causing a blockage. However, slowly increasing the amplitude alleviates the blockage phenomenon. When high-viscosity materials are subjected to high-intensity acoustic vibration, the flow field is dominated by shear flow, which is accompanied by efficient stretching and folding. Changing the amplitude or frequency alone can cause blockage, and increasing the frequency of vibration excitation alone will not alleviate the blockage. Instead, increasing the amplitude can generate more mixing-promoting reflux, effectively relieving blockage while maintaining stable conveying capacity.

Keywords: Acoustic Frequency Vibration; Continuous Mixing; High Viscosity Fluid; Conveying; CFD

1. Introduction

Mixing is a critical process in numerous industries, where homogeneity in the product mixture is essential for further manufacturing processes. Traditionally, mixing has been performed in batch mode, which ensures accurate feeding and reliable quality control. However, scaling up this method has limitations and frequent manipulations are necessary during the operation. To address these challenges, in recent years, continuous mixing processes have been developed. These processes allow for efficient continuous mixing, while conveying materials, and offer several advantages, including reduced processing time and increased efficiency for large-scale production.[1]

Continuous mixing process can achieve the homogeneity of the components while conveying the material, thereby enhancing mixing efficiency and reducing the time consumed by stopping, loading and unloading.[2] This approach has found wide applications in the chemical, food and pharmaceutical industries,[3] where efficient and precise mixing is essential for product quality. The viscosity characteristics of fluids are a major determinant of the mixing and conveying efficiency of continuous mixing systems, making it a critical factor in their performance.[4] In various types of production practices, mixing high viscosity fluids can be challenging, as these fluids lack the turbulence and diffusion assistance necessary for efficient mixing,[5,6] resulting in difficulties in achieving continuity.

Twin-screw extrusion is currently the most commonly used continuous mixing method, and has been extensively studied with regard to its manufacturing, performance, and theory.[7-9] However, due to the presence of paddle kneading in twin-screw extrusion, the mixing of flammable and explosive substances is hazardous. To address this issue, Tran-Minh, Dong and Karlsen [9] proposed an elliptical planar micro-mixer that operates passively in a laminar flow state and is suitable for lower viscosity

substances. Oshino, Nishihama, Wakamatsu, Inoue, Matsui, Okui, Nakajima, Kuniyoshi and Nakamura [10] developed a peristaltic continuous mixing device that operates like an intestinal tract using pneumatic artificial muscles made of soft rubber material. Although this device can be used for mixing high viscosity substances, related research is still in its early stages. Continuous mixing technology offers numerous advantages, which make it a hot topic in both industrial and academic research. As a result, various implementation methods have been proposed repeatedly, highlighting the importance of this technology in different fields.

The flow properties of fluids under acoustic vibration excitation are complex, with phenomena such as the generation of Faraday waves.[11] Kumar and Tuckerman [12] derived an equation for the stability of the interface between two viscous fluids under the influence of vertical sinusoidal force and performed Floquet analysis. Hashimoto and Sudo [13] investigated the kinetic behavior of two fluids with free surfaces in a vessel subjected to vertical vibrations, and analyzed the stability of the free surfaces and interfaces of two fluids with different densities. Ito and Komori [14] proposed a vibration technique to enhance fluid mixing and chemical reactions in microchannels. Their experimental results demonstrated a significant improvement in fluid mixing and chemical reactions. Additionally, Resodyn, USA, has developed an acoustic resonance mixing technique.[15] This method utilizes mechanical resonance to generate high-intensity mechanical vibration, promoting fluid flow within the mixing vessel.[16] Qu, Yi and Guan [17] conducted relevant simulations on acoustic resonance technology, analyzing and determining the relationship between vibration parameters, material properties, and the final mixing effect. They found that increasing frequency and amplitude can significantly enhance the mixing efficiency. Vandenberg and Wille [18] conducted relevant research on acoustic resonance mixing technology for high-

performance concrete, comparing it with conventional paddle mixing and examining differences in mixing performance in terms of fluidity, compressive strength, and bending strength, among others. Zhang, Zhan, Zhang, Hou and Li [19] applied the acoustic resonance continuous mixing technique to the preparation of nano-TATB, and the experiments and simulations demonstrated that the technique could significantly improve the mixing efficiency of the fluid in the microreactor.

Vibratory transport has also received significant attention and research. Numerical results from Bouarab, Mokhtari, Kaddeche, Henry, Botton and Medelfef [20] indicate that the flow can be amplified or damped depending on the direction of vibration, and critical vibration angles may even cause flow reversal. Kipriyanov and Savinykh [21] revealed the degree of influence of vibration amplitude on the conveying speed of grain materials, and obtained a mathematical model of amplitude change depending on the operating mode and settings of the vibratory conveying machine.Chen, Jiang, Shen, Weiwei and Li [22] proposed a harmonic horizontally vibratory conveying method based on a vibrating plate with zigzag morphology and the results showed that unidirectional conveying occurs when the vibration strength exceeds a certain value.

Acoustic vibration is an effective method to drive rapid directional flow of fluids and enhance convection between fluids with density gradients. Acoustic frequency vibration excitation is also a viable option for achieving continuous flow mixing processes. In recent years, Resodyn, a US-based company, has developed a continuous mixing system based on an acoustic resonance mixer to explore the continuous transport and uniform dispersion of materials under 60 Hz vibration excitation. At present, the research on continuous mixing of high-viscosity fluids under acoustic frequency vibration excitation is still limited to the public, and the characteristics of the mixed

flow field in the continuous mixing process have not been fully elucidated. The influence of process parameters such as frequency, amplitude, and their combination on mixing and conveying efficiency under acoustic frequency vibration is not yet fully understood. This knowledge gap currently limits the widespread application and further development of continuous mixing technology using acoustic frequency vibration.This paper presents a CFD simulation model to investigate the continuous mixing process of high viscosity materials under acoustic vibration excitation. The model is validated through experiments, and the continuous conveying and mixing characteristics of high viscosity materials are analyzed. Furthermore, the paper qualitatively and quantitatively describes the mixing and conveying effects under different vibration parameters, and elucidates the mechanism of acoustic resonance continuous mixing, which can promote its application in high viscosity fluids.

2. Experimental setup and simulation model

2.1. Experimental setup

The experimental setup for acoustic vibration continuous mixing is depicted in Figure 1. The continuous mixing flow channel is mounted on a vertical vibration platform capable of generating controlled vibrations with amplitudes ranging from 0.5 to 10 mm and frequencies ranging from 1 to 100 Hz, with control accuracy within ±0.2 mm and ±0.5 Hz, respectively. A piezoelectric accelerometer is employed to measure the vibration frequency and amplitude. A high-speed camera is positioned to capture the mixing process, providing high-definition photography under high-frequency vibration.

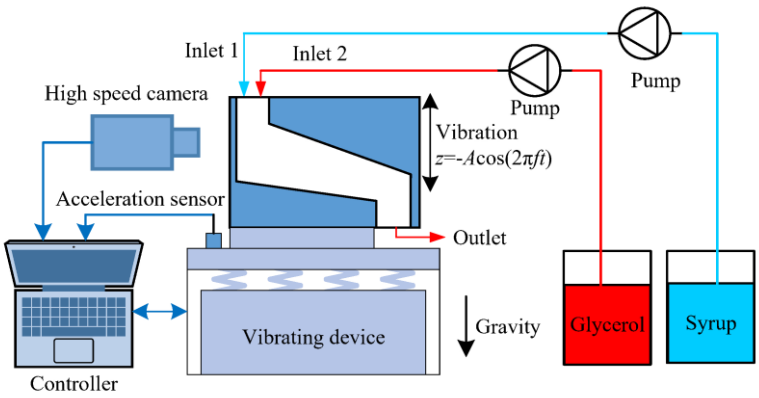

Figure 1. Schematic diagram of the continuous mixing system of acoustic frequency vibration

The continuous mixing flow channel is mounted on a mechanical vibration platform that applies high intensity mechanical vibration in the vertical direction to the vessel. To simplify the subsequent analysis and express the velocity equation as a sinusoidal function without an initial phase, the vibration displacement equation can be set as

$$z = -A\cos(2\pi ft) \tag{1}$$

Differentiating the above equation with respect to time, the vibration velocity equation of the vessel is obtained as follows:

$$v = \frac{dz}{dt} = 2\pi fA\sin(2\pi ft) \tag{2}$$

By differentiating the vibration velocity, the vibration acceleration equation of the vessel is obtained as follows:

$$a = \frac{d^2z}{dt^2} = 4\pi^2 f^2 A\cos(2\pi ft) \tag{3}$$

Where the wave phase is $\varphi=2\pi ft$ and the wave period is $T=1/f$.

To facilitate observation, the continuous mixing vessel is constructed from transparent acrylic sheet, with the dimensions and boundary conditions shown in Figure

2. The vessel has inlet and outlet connected to atmospheric pressure, and the inlets features two square inlets Inlet1 and Inlet2, each with a side length of 8 mm and symmetrically distributed in the plane. These inlets can be used to supply the two component liquids, respectively. The syrup and glycerol are fed to the two inlets via a dosing pump at a mass flow rate of 1:1, following the set flow rate. The vessel and the material are situated in an atmospheric environment at a temperature of 20 °C. The relevant material parameters are presented in Table 1.

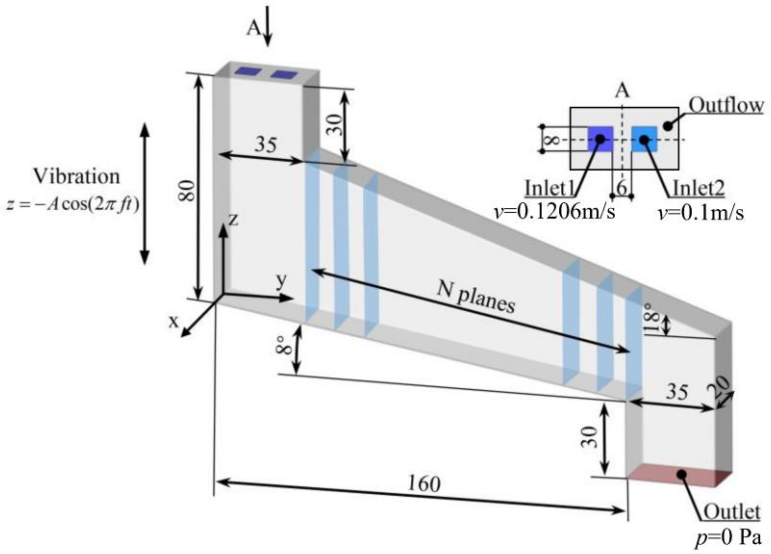

Figure 2. Geometry and boundary conditions of continuous mixing vessel

Table 1. Material parameters

Matter	Density (kg/m^3)	Viscosity (Pa-s)	Diffusion coefficient (m^2/s)	Surface tension coefficient with space (N/m)	Mass flow rate (g/s)	Inlet flow rate (m/s)
Air	1.225	1.8×10^{-5}	-	-	-	-
Syrup	1045	1.12	1.24×10^{-9}	0.0717	6.4512	0.0965
Glycerin	1260	1.41	1.24×10^{-9}	0.0636	6.4512	0.08

2.2. Control equations and boundary conditions

The simulation model studied in this paper deals with two-phase flow of gas and liquid, where the gas phase and the liquid phase are immiscible, while the liquid phase is composed of two intermixable liquids. The Volume of Fluid (VOF) model is employed to capture the changes in the free surface between the immiscible gas phase and the liquid phase.[23] In this study, the VOF model is utilized to simulate the unmixable gas-liquid two-phase flow. For two mutually soluble liquids in the liquid phase, the VOF model tracks the gas-liquid interface by solving the continuity equation for the volume fraction of each phase,[24] which takes the form

$$\frac{\partial c_i}{\partial t} + \nabla c_i \boldsymbol{U}_i = 0 \tag{4}$$

The momentum equation for each phase [24] is

$$\frac{\partial \rho_i \boldsymbol{U}_i}{\partial t} + \nabla(\rho_i \boldsymbol{U}_i \boldsymbol{U}_i) = -\nabla p + \nabla\left[\mu_i\left(\nabla \boldsymbol{U}_i + \nabla \boldsymbol{U}_i^T\right)\right] + \rho_i \boldsymbol{g} + \boldsymbol{S} \tag{5}$$

The sum of the volume fractions of each phase is

$$\sum_{i=1}^{n} c_i = 1 \tag{6}$$

where c_i denotes the volume fraction of each phase; $\boldsymbol{U}_i$ denotes the velocity vector of each phase; ρ_i denotes the density of each phase; μ_i denotes the viscosity of each phase; and $\boldsymbol{S}$ is the volume force source term due to surface tension; the subindex i = 1, 2, denotes the air phase and liquid phase, respectively. The volumetric force source term $\boldsymbol{S}$ is modeled using the continuous surface tension.[25] This captures the effect of surface tension in the phase interface by calculating the surface tension as a volumetric force source term $\boldsymbol{S}$ based on the dispersion theorem. In addition, the material is assumed to be incompressible and isothermal, and there is no involvement of the energy

conservation law. Furthermore, the mixing process is assumed to involve no chemical reactions.

The component transport model can be utilized to describe the mixing process of two mutually soluble liquids in the liquid phase.[26] In this study, the component transport model is employed to model the mutual solubility properties of two liquids. The component transport equation between liquids [24] is

$$\frac{\partial \rho_{2,j} c_{2,j}}{\partial t} + \nabla(\rho_{2,j} c_{2,j} \boldsymbol{U}_{2,j}) = I \nabla^2 c_{2,j} \tag{7}$$

where $\rho_{2,j}$ denotes the density of each component in the liquid phase; $c_{2,j}$ denotes the volume fraction of each component in the liquid phase; $\boldsymbol{U}_{2,j}$ denotes the velocity vector of each component in the liquid phase; I is the diffusion coefficient; and j = 1,2, for the two liquids.

The density and viscosity of the liquid phase are determined, respectively, by the volume-weighted mixing method and the mass-weighted mixing method of the components, i.e.

$$\rho_2 = \frac{1}{\sum_{j=1}^{n} c_{2,j} / \rho_{2,j}} \tag{8}$$

$$\mu_2 = \sum_{j=1}^{n} c_{2,j} \mu_{2,j} \tag{9}$$

where $\mu_{2,j}$ indicates the viscosity of the components in the liquid phase.

To achieve the effect of vibration mixing in the special case of grid motion, the slip grid technique can be used.[27] In this paper, a slip-grid model is implemented to apply the vibration, such that the wall motion of the container becomes a function of the velocity described in (2). This model is able to describe a moving mesh scenario where the mesh nodes make rigid motions within a specific region of the moving mesh. The

conservation equation in integral form for a generic scalar ϕ on a control body V with boundary motion and a moving grid can be written as:

$$\frac{d}{dt}\int_V \rho\phi dV + \int_{\partial V} \rho\phi\left(\boldsymbol{U} - \boldsymbol{U}_g\right)\cdot d\mathrm{B} = \int_{\partial V} \Gamma\nabla\phi\cdot dA + \int_V S_\phi dV \qquad (10)$$

where ρ is the fluid density; $\boldsymbol{U}_g$ is the grid velocity of the moving grid; Γ is the diffusion coefficient; S_ϕ is the source term of ϕ; B is the control surface area; and ∂V is used to describe the control body boundary.

In vibratory continuous mixing, the Reynolds number of the liquid phase is calculated using the equation $Re = 2\pi\rho Af\mathrm{D}/\mu$, where D is the equivalent diameter. For the range of vibration frequencies, vibration amplitudes, and inlet flow rates used in this study, the Reynolds number is always less than 250, which indicates laminar flow. Therefore, a laminar flow model simulation is used.[28] Figure 2 shows a local view in the A-direction, which illustrates the placement of velocity inlet boundaries Inlet1 and Inlet2 in the plane. The rest of the area is set as the Outflow boundary, which allows air to enter and exit freely. The outlet is set as a pressure outlet boundary at 0 Pa, and the rest of the boundary is set as a no-slip Wall.

2.3. Meshing and solution independence

The geometry was meshed using ICEM software with a hexahedral mesh type. To ensure mesh independence, a preliminary mesh convergence study was conducted. Two criteria were used: the first outflow time elapsed from t = 0 s until the liquid phase first reaches the outlet, and the outflow mass of the liquid phase from the outlet in the period from t = 0-25 s, for vibration parameters of f = 60 Hz and A = 4 mm. Figure 3 presents the results for different grid sizes. Both parameters exhibited differences of less than 5.0% when the number of grids exceeded 600,000. Thus, a grid number of 600,000 can be chosen to ensure reasonable accuracy and a suitable calculation scale.

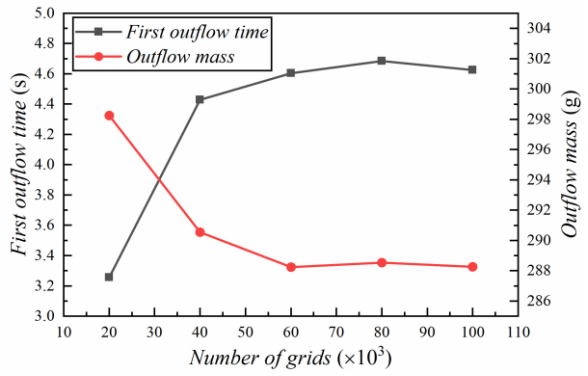

Figure 3. Grid-independent verification

2.4. Experimental verification

To assess the accuracy of the computational model, the experiments were conducted using syrup (marked in red) and glycerin (marked in blue) with the properties outlined in Table 1. The experimental data were compared with the simulations results for corresponding parameters, which included waveforms at the gas-liquid interface for vessel vibration frequencies of f = 40 Hz and various amplitudes, as well as the first outflow time and the outflow mass of the liquid phase from the outlet within the time range t = 0-25 s. The inlet flow rate for Inlet1 was set to 0.048 m/s, while Inlet2 was set to 0.04 m/s, and the mass flow rate was 3.2 g/s.

Figure 4 depicts the flow field pattern inside the container, as qualitatively compared through the gas-liquid interface obtained from both experimental and simulated data. By examining the shape of the simulated free surface, it is apparent that the number and amplitude of the ripples at the gas-liquid interface increase with higher vibration amplitudes A, which agrees well with the experimental observations.

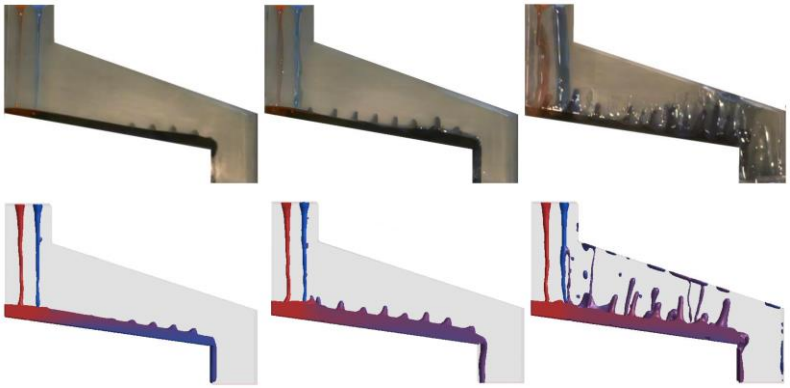

Figure 4. Experimental liquid level fluctuation (upper) and simulated liquid level fluctuation (lower) with f = 40 Hz and different A.

Figure 5 shows the quantitative verification of simulation accuracy. The error between the simulated and experimental values for the first outflow time and outflow mass is within 8%, indicating that the simulation results can accurately reflect the flow characteristics.

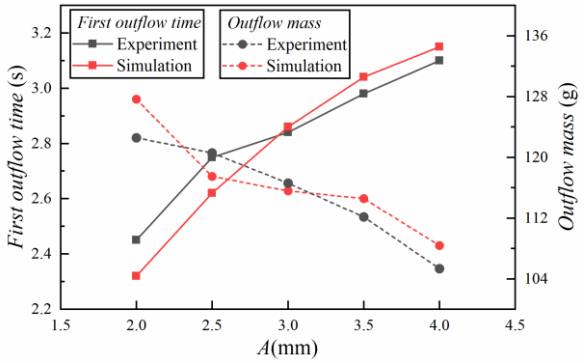

Figure 5. Comparison of the first outflow time and the outflow mass between experiment and numerical simulation was conducted at f = 40 Hz and different A.

2.5. Evaluation Indicators

In this study, Inlet1 and Inlet2 had equal mass flow rates, resulting in an ideal mixing outcome for the two-component liquid where the glycerol mass fraction at each sampling point in the liquid phase region was x_i = 50%. To better understand the mixing characteristics of the two-component liquid and evaluate the gap between the mixing uniformity at each sampling point in the mixer vessel and the desired ideal mixing

result, this study uses the Relative Standard Deviation (RSD) [29] of the mixing concentration and the uniform mixing concentration for evaluation, which is calculated as follows

$$RSD_M = \frac{1}{50\%}\sqrt{\frac{1}{n-1}\sum_{i=1}^{n}\left(x_i - 50\%\right)^2} \tag{11}$$

Where x_i is the mass fraction of glycerol measured at n sampling points in the liquid phase region, at a certain time during the mixing process, and RTD_M is the average mass fraction of glycerol across all sampling points in the liquid phase.

The system's conveying performance is assessed through the mean residence time RTD_{avg}, i.e., the average time that a fluid micro-element spends in the vessel from inlet to outlet.[30] Calculations were performed using discrete data

$$RTD_{avg} = \sum_{i=1}^{m} t_i E(t_i)\Delta t_i \Big/ \sum_{i=1}^{m} E(t_i)\Delta t_i \tag{12}$$

Where, $E(t_i)$ is the density function of residence time distribution, represents the percentage of total material that has been resident for a certain time t_i, m is the number of sampling moments, and satisfies $\sum_{i=1}^{m} E(t_i)\Delta t_i$ equal to 1.

When subjected to vibration excitation, some of the fluid in the vessel flows in a backward direction, forming backflow. To quantify the extent of backflow in the flow field, the average backflow coefficient is used as an evaluation metric. The reflux coefficient is defined as the ratio of the return flow rate to the net flow rate in a cross section perpendicular to the flow direction.[31] The average reflux coefficient, denoted by G_{avg}, is calculated as the average of the reflux coefficients obtained from N vertical cross sections within one cycle T,

$$G_{avg} = \sum_{l=1}^{N}\sum_{k=1}^{m}(Q'_{l,k} / Q_{l,k}) / (NT) \tag{13}$$

where the number of cross sections N is set to 26 and are equally spaced and vertically distributed. The sampling moments k, with k = 1,2,.., m, are chosen in the first cycle T, and l denotes the l-th surface. Q and Q' denote the net flow rate and the return flow rate, respectively, where the positive direction of the y-axis indicates the flow direction. The distribution area of the cross sections is illustrated in Figure 2.

To understand fluid mixing, one can consider it as interfacial stretching. Different types of flows have varying effects on interfacial stretching, leading to varying potential mixing capacities or mixing efficiencies. To differentiate between flow types and evaluate the potential mixing capacity of the flow field, a mixing index α is commonly used as a quantitative measure.[32] The mixing index is defined as follows

$$\alpha = \frac{\sqrt{\boldsymbol{D}:\boldsymbol{D}}}{\sqrt{\boldsymbol{D}:\boldsymbol{D}}+\sqrt{\boldsymbol{\Omega}^{T}:\boldsymbol{\Omega}}} \tag{14}$$

Where $\boldsymbol{D}$ denotes the deformation rate tensor; and $\boldsymbol{\Omega}$ denotes the vorticity tensor. The mixing index α is used to distinguish the flow type and assess its potential mixing capacity: α = 1 denotes pure tensile flow; α = 0.5 denotes pure shear flow; α = 0 denotes pure rotational flow. Therefore, a larger value of α indicates a higher proportion of tensile flow and a higher ability of dispersed mixing under the same conditions. The average mixing index $\bar{\alpha}$ is obtained by calculating the arithmetic mean of the mixing index α for all grid nodes on the object being analyzed.

3. Results and discussions

3.1. Process of mixing and flow induced by forced vibration

At the initial moment t = 0 s, the liquid is introduced into the continuous mixing vessel through the Inlet1 and Inlet2, respectively, and the acoustic vibration excitation is applied. The initial stage of a continuous mixing processes is complex, but the stabilized state reflects the actual mixing and conveying characteristics more accurately. The

steady state is defined as the point at which the change in RSD_M at the outlet (Outlet) becomes less than 0.1 and t > 30 s, after which the flow states at the same vibration phase are similar. At the vibration phase around φ = 90°, the fluid exhibits significant characteristics. Therefore, the flow field is analyzed and compared at a vibration phase of 90° after stabilization.

In the absence of vibration (i.e., vibration intensity is 0), the two-component liquid is subject to natural flow. The concentration and velocity fields at steady state are depicted in Figure 6. Since there is no vibration, the velocity gradient between the two liquid phases is not noticeable, resulting in the formation of a dividing line between the liquid-liquid phases. Furthermore, there is an evident mass concentration gradient at the outlet of the vessel, and some bubbles are mixed in the liquid phase. Once the vibration is initiated, the motion pattern of the liquid undergoes significant changes under different vibration amplitudes, giving rise to three typical mixing and flow processes as follows.

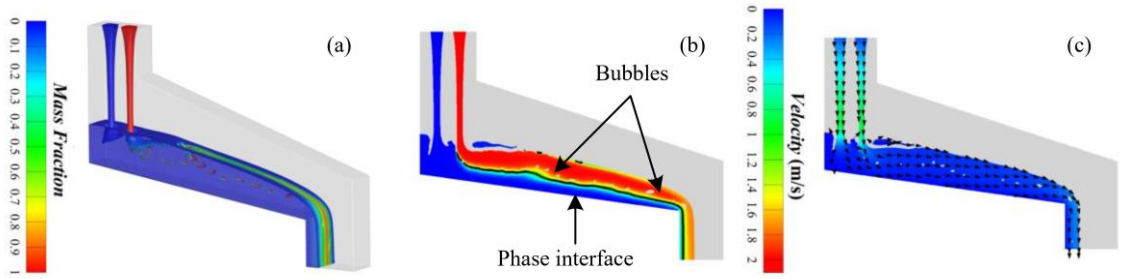

Figure 6. (a) 3D mass concentration field without vibration applied; (b) YZ cross-section mass concentration field; (c) YZ cross-section velocity field.

At low vibration intensity, the two-component liquid can be effectively conveyed, the transport is normal, and the mass concentration gradient at the vessel outlet is greatly reduced compared to when no vibration is applied. Under the vibration excitation of A=3.5 mm, periodic standing waves (faraday waves) appear on the smooth free surface while the velocity field in the bottom region remains relatively stable

(Figure 7c and f). This enhances the mixing effect near the free surface only (Figure 7b and e), with the phase interface remaining stable. However, as shown in Figure 7g-i, increasing the amplitude leads to intensified deformation of the free surface, making the velocity field in the nearby area turbulent and causing the standing wave to gradually take on an irregular form. This produces jets in the form of liquid columns, some of which are stripped from the free surface or ejected to the upper surface of the vessel. The phase interface of the two-component liquid begins to deform, and the degree of deformation of the phase interface is much smaller than that of the free surface, which indicates that the two-component liquid phase interface has a slightly higher deformation threshold than the free surface. The deformation of the phase interface can lead to an increase in the contact area between the two-component liquids, which in turn promotes mixing. As shown in Figure 7i, the deformation of the free surface generates multiple circulating convection flows that extend from the free surface towards the interior of the liquid phase. These convection flows effectively enhance the mixing effect.

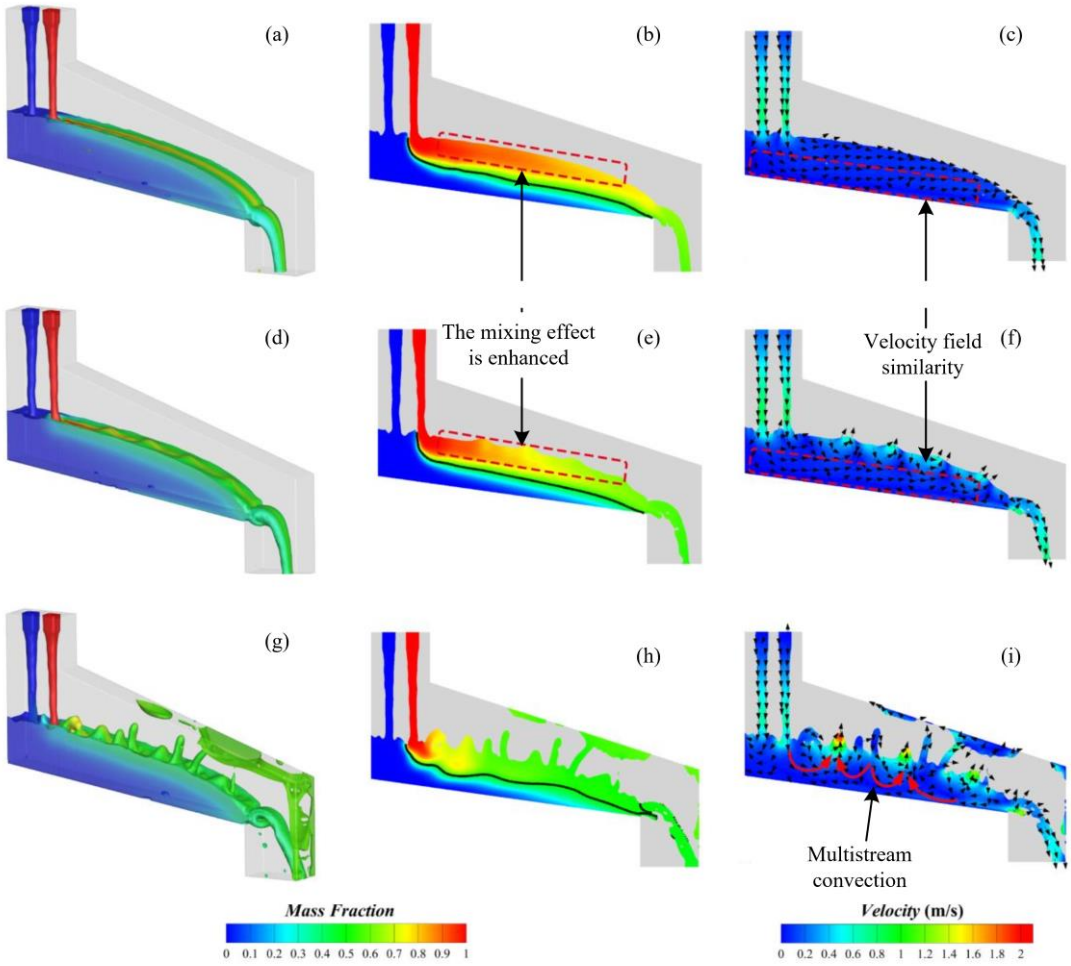

Figure 7. Three-dimensional mass concentration field (left), YZ cross-section mass concentration field (middle) and YZ cross-section velocity field (right) at a vibration frequency of 60 Hz with different amplitudes at low vibration intensity of f = 60 Hz. (a-c) A = 3 mm.(d-f) A = 3.5 mm. (g-i) A = 4 mm.

As the vibration intensity increases, the flow of the two-component liquid is hindered, and the liquid gradually fills up most of the container, leading to changes in the concentration and velocity fields over time, as shown in Fig. 8. At the initial stage, the more intense vibration causes the free surface to deform further, resulting in the formation of narrower columnar jets. Simultaneously, the distance between the upper and lower walls of the vessel flow channel decreases as the liquid flows inside the vessel, causing the jets to reach the upper surface of the vessel more easily, as shown in Figure 8a and b. Some of the jets detach from the free surface and adhere to the upper

surface downstream of the vessel runner, while the un-detached jets connect the fluids on the upper and lower surfaces, forming a "barrier" that hinders the flow of the liquid phase towards the outlet. This impediment causes the liquid phase to accumulate at the outlet and fill upstream, as illustrated in Figure 8c, d. As the buildup reaches a certain level, the system attains a steady state, as shown in Figure 8e, f.

In the velocity field cloud map Figure 8f, it can be observed that the downstream liquid phase in the vessel is divided into two streams: one stream faces the outlet, but its velocity direction is oriented at an angle to the lower surface, while the other stream produces a backflow effect. The reflux effect, on one hand, can help to enhance mixing between the components and reduce the uniformity change caused by the fluctuation of the filling. However, at the same time, it can also slow down the rate of transport, and even cause fluid to be unable to discharge, leading to blockage in the flow channel. The two flow directions keep the filling rate of the liquid in the container consistently high, but also hinder the flow of liquid, producing the effect of blockage, and increasing the retention time of the liquid in the container.

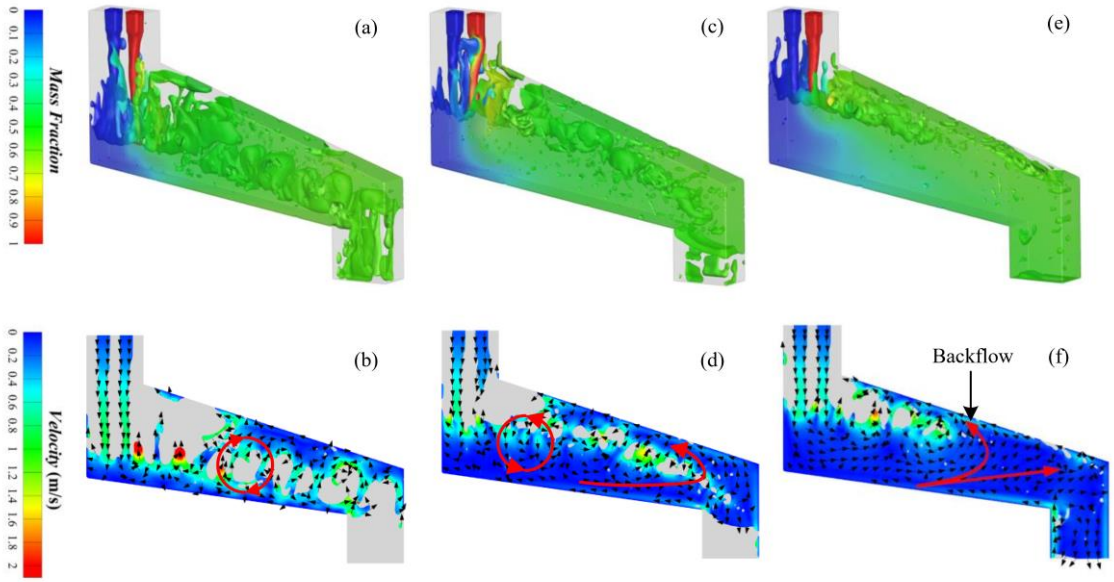

Figure 8. Three-dimensional mass concentration field (top), YZ cross-sectional velocity field (bottom) at different t for f = 60 Hz and A = 5 mm vibration intensity. (a-b) t = 10 s. (c-d) t = 20 s. (e-f) t = 40 s.

By increasing the intensity of vibration further, the liquid blockage in the container can be effectively relieved. As shown in Figure 9c2, high-intensity vibration imparts a large kinetic energy to the liquid, resulting in a jet velocity greater than 2 m/s. This helps the liquid to overcome the viscous force and disperse rapidly in the vessel, keeping the flow channel open. In comparison to the vibration intensity of f = 60 Hz, A = 5 mm, the high intensity vibration prevents local accumulation of materials and reduces the amount of liquid mixed in the container. The flow state at 60 Hz and 6 mm amplitude, as shown in Figure 9, achieves good mixing effect and also avoids liquid blockage, which improves the safety of mixing and equipment stability. In addition, the high intensity vibration increases the number of jets in the flow region, accompanied by more efficient stretching, shearing and folding. This serves as a stirring mechanism that significantly enhances the mixing effect.

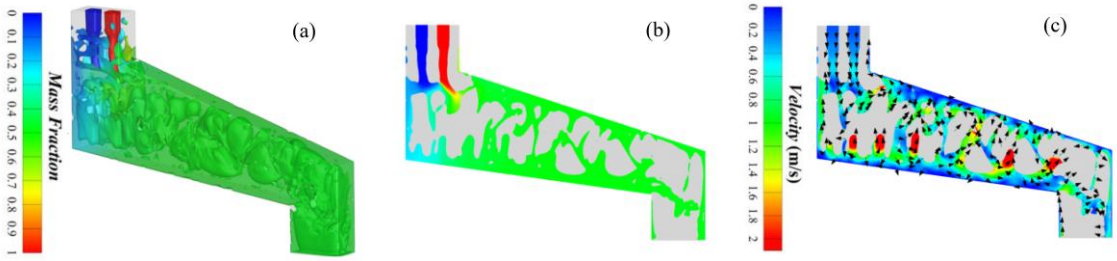

Figure 9. (a) 3D mass concentration field, (b) YZ cross-section mass concentration field, (c) YZ cross-section velocity field for φ = 90° at high intensity vibration intensity of f = 60 Hz, A = 3 mm.

3.2. Evaluation of mixing type and shear environment

The flow field of the liquid phase under three different process parameters (A = 4, 5, and 6 mm at f = 60 Hz) exhibits three distinct flow field states. As shown in Figure 10, the mixing index $\bar{\alpha}$ of the liquid phase fluctuates over three cycles, then the flow reaches a steady state at all three process parameters. The mixing index under vibration fluctuates periodically with a period of about 0.5T. When the amplitude is increased from 4 mm to 5 mm, $\bar{\alpha}$ becomes larger, indicating an increase in the tensile flow in the vessel. However, when the amplitude is increased to 6 mm, $\bar{\alpha}$ decreases greatly, which indicates a decrease in the shear flow field.

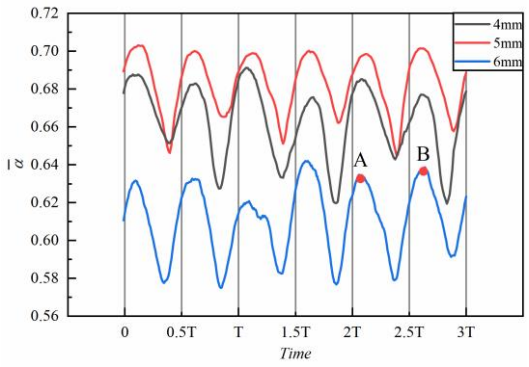

Figure 10. Variation curves of the liquid phase in the flow field for 3T at f = 60 Hz and A = 4, 5, 6 mm vibration intensity $\bar{\alpha}$

The process parameters of f = 60 Hz and A = 6 mm result in efficient mixing without any blockage in the vessel, which is an ideal mixing situation. Figure 11a and b show the velocity field and mixing index at Point A and Point B (as shown in Figure 10), located at about 30° phase of sine function, where the vessel is accelerating in the positive direction. Due to the effects of inertia and other factors, the liquid phase produces a downward velocity field relative to the direction of vessel motion. This results in the liquid phase above the vessel stretching downward, generating a small amount of efficient stretching flow. The liquid phase below the vessel is compressed downward, which causes the liquid phase to spread in all directions along the wall, also forming a small amount of tensile flow. At the same time, the stretching motion of the liquid phase below the vessel in all directions generates multiple convection flows, which promote the mixing effect, and their tendency to move upward allows the liquid phase to produce an upward ejected liquid column in the subsequent motion.

The peak shown in Figure 11b is observed at approximately 223° phase of the velocity sine function, corresponding to when the vessel is moving in the negative direction. Due to multiple convection flows generated by the liquid phase under the previous motion, as shown in Figure 11a, and the inertia effect, the liquid phase generates an upward velocity field with respect to the direction of vessel motion, leading to the formation of more upward ejected liquid columns. As a result, the liquid phase below the vessel stretches upward, producing a large number of efficient stretching flows. On the other hand, the liquid phase above the vessel is compressed against the wall, which has a large inclination, forming only a unidirectional return flow along the wall and a large amount of tensile flow, similar to Figure 11a. These refluxes, promote the mixing effect and tend to move downward, together with the inertia effect, allowing the liquid phase to produce a downward ejected liquid column in the

subsequent motion (Figure 11a). This process repeats in vibration, causing the mixing index to fluctuate approximately as a sinusoidal function with a period of about 0.5*T* and providing the acoustic resonance continuum device with its efficient mixing capability. The efficient tensile flow is mainly present in the interior of the liquid phase, while the shear flow dominates the gas-liquid free surface and the region near the contact between the liquid phase and the wall.

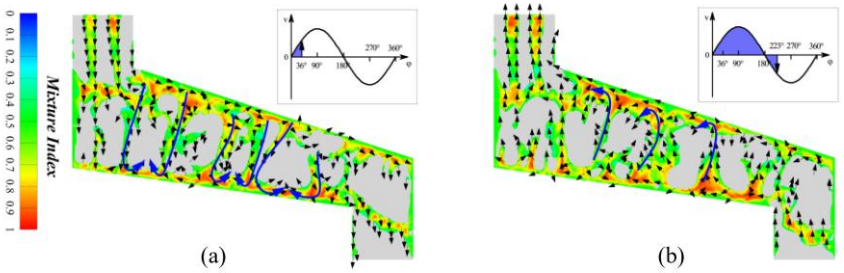

Figure 11. α cloud diagram of the liquid phase of the YZ cross section, (a) Point A; (b) Point B.

The probability distribution curves of α for the liquid phase were analyzed at the peak point and near the trough moment for the three process parameters of A = 4, 5 and 6 mm at f = 60 Hz, as shown in Figure 12. It can be observed that the α probability distribution is similar for all cases, with the peak of the curve occurring at about 0.5, and α *is* mainly concentrated around 0.45-0.65, while it is almost null on 0-0.35. This indicates that the flow field of the acoustic resonance mixer is primarily dominated by shear flow, with a small amount of tensile flow, and the presence of rotational flow is relatively weak.

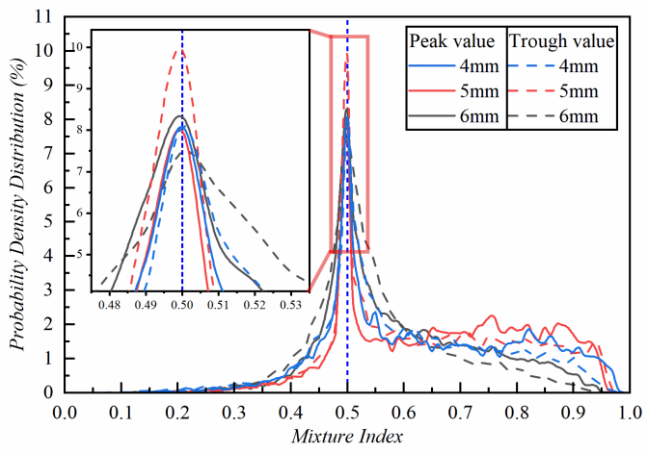

Figure 12. Probability distribution curves of α at the peak and trough points

3.3. Effect of vibration parameters on mixing and flow

In order to compare mixing at different amplitudes in steady state, the homogeneity of different cross sections in the flow channel was analyzed. Figure 13 shows the RSD_M *at* the same moment on different positioned cross sections of the vessel flow channel after the flow field reaches steady state with φ = 90°, and the monitoring planes within the flow channel are set as in Figure 2. The overall mixing uniformity tends to improve as the flow proceeds (see Figure 13), and the RSD_M obtained under the action of vibration has a significant decrease compared to the case without vibration. Among them, the amount of RSD_M curve fluctuation increases after the amplitude reaches 4 mm, which is caused by the increased deformation of the free surface of the liquid phase in the mixing vessel and the appearance of a large number of jets. Some of the less mixed jets may fall to the downstream region or they may adhere to the upper wall surface of the vessel, resulting in little change in RSD_M in the downstream cross-section region of the vessel compared to the upstream or even appearing larger than the RSD_M in the upstream cross-section. After the amplitude is greater than 5.5 mm, the fluctuation of the RSD_M curve is more significant because the liquid phase in the mixing vessel reaches the full-

field dispersion under high-intensity vibration, making the above phenomenon more pronounced.

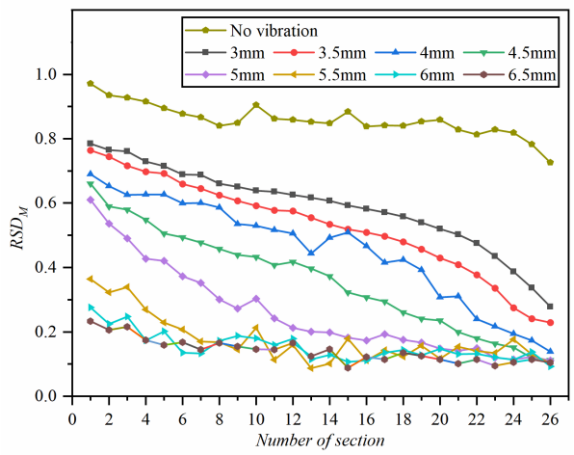

Figure 13. RSD_M of liquid phase for no vibration and different amplitudes at f = 60Hz in the cross section of the vessel flow channel for φ = 90°

By examining the RSD_M at the starting interface (*Number of section* =1) for each amplitude, it was observed that the amplitude varies the most between 5 mm and 5.5 mm, which is attributed to the formation of an ideal mixing state similar to Figure 9. This state effectively enhances the mixing capacity. At the end interface (*Number of section* = 26), the RSD_M was analyzed for each amplitude, and it was found that it decreased with increasing amplitude from 3 mm to 4 mm. However, for amplitudes of 4.5 mm and above, the RSD_M remains stable at around 0.1. This indicates that a certain threshold of amplitude is necessary to achieve uniform mixing of two-component high-viscosity liquids.

After reaching a steady state, Figure 14 displays the RTD_{avg} and G_{avg} curves for various amplitudes at 60 Hz. It is evident that as the amplitude increases below 5.5 mm, the RTD_{avg} rises rapidly. However, as the amplitude continues to increase beyond 5.5 mm, the growth of RTD_{avg} starts to slow down. This is because before the amplitude of 5.5 mm, the reflux of the liquid phase and the increase in RTD_{avg} become more significant as the amplitude increases. After 5.5 mm, the liquid phase can be dispersed

rapidly under high intensity vibration, relieving the blockage of the liquid phase in the vessel. As a result, the RTD_{avg} does not continue to increase rapidly with an increase in amplitude.

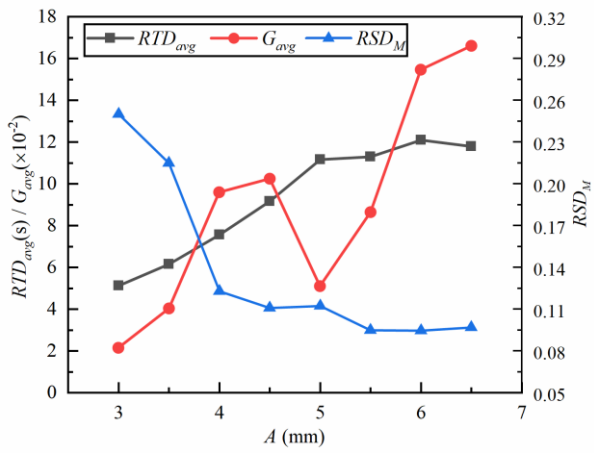

Figure 14. RTD_{avg} for different A at f = 60Hz, G_{avg} at φ = 90° and RSD_M at Outlet

The G_{avg} curve shows an initial increase with increasing amplitude, followed by a decrease, and then another increase. This behavior can be attributed to the fact that as the amplitude increases within the 4-5 mm range, the blockage of the liquid phase in the vessel becomes more severe, resulting in a higher filling rate of the liquid phase in the vessel and a lack of spare space to produce reflux. However, when the amplitude is increased beyond 5 mm, the liquid phase is rapidly dispersed, leading to a decrease in the filling rate of the liquid phase inside the vessel and an enhancement in the reflux effect, which in turn increases G_{avg}. In the tested range of A, there was a roughly negative correlation between RSD_M and RTD_{avg}, while there was no significant relationship between RSD_M and G_{avg}.

Figure 15 shows the variation of the RSD_M of the liquid phase at the same moment in the cross section set up in the vessel flow channel at different frequencies with an amplitude of 4 mm and phase φ = 90°. It can be observed from Figure 15 that the RSD_M at the end interface (*Number of section* = 26) decreases by about 65% at 40 Hz compared to the case without vibration. The overlap of the RSD_M curves at 50 Hz,

60 Hz and 70 Hz is significant, indicating that the increase in frequency does not bring about a significant mixing effect. This is due to the fact that the increase in frequency leads to an increase in the agglomeration and blockage of the liquid phase in the vessel, making it impossible to achieve full-field dispersion in the mixing vessel.

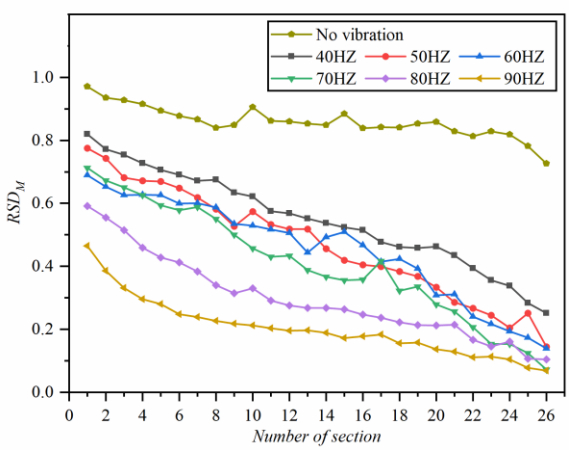

Figure 15. RSD_M of the liquid phase at φ = 90° for different f without vibration and A = 4 mm over the cross section of the vessel flow channel

The RTD_{avg} increases with the amplitude, unlike the case shown in Figure 14. This is because higher vibration frequencies results in more significant liquid phase agglomeration and blockage in the vessel. The G_{avg} curve increases and then decreases with the amplitude. This is also due to the blockage of the liquid phase inside the vessel, resulting in a lack of space to generate reflux when the frequency increases between 70-90 Hz (as shown in the 60 and 90 Hz flow patterns in Figure 16). In the f range tested, RSD_M and RTD_{avg} exhibit a negative correlation, whereas RSD_M and G_{avg} show no significant relationship. Furthermore, a minimum threshold value of about 0.08 exists for RSD_M at Outlet, which is similar to the situation at f = 60 Hz for different amplitudes.

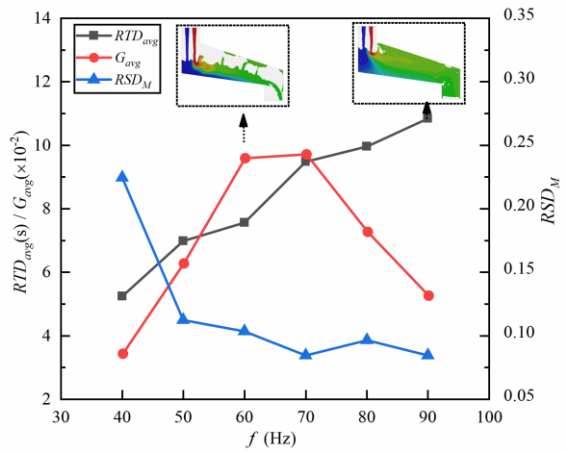

Figure 16. RTD_{avg} at different f for A = 4mm, G_{avg} at φ = 90° and RSD_M at Outlet

The mixing process is significantly influenced by both frequency and amplitude. In order to further investigate their effects, the mixing behavior was analyzed for various combinations of frequency and amplitude at an acceleration value of 588 m/s^2. The specific parameter combinations tested are outlined in Table 2.

Table 2. Combinations of a = 588 m/s^2 , different A and f

Work Condition	A (mm)	f (Hz)
a	2	86.3
b	3	70.5
c	4	61.0
d	5	54.6
e	6	49.8
f	7	46.1

Figure 17 illustrates that, even when using the same acceleration value, the mixing effect can vary significantly for different combinations of amplitude and frequency. Under high frequency and low amplitude conditions (condition b in Figure 18), a large number of surface waves are produced on the liquid surface, which keeps the liquid phase in a fluctuating state and results in low mixing capacity. This is similar to the vibration parameters of f = 60 Hz and A = 3.5 mm, as shown in Figure 7d-f. On

the other hand, the mixing quality is significantly higher in the case of high amplitude at low frequencies than that in the case of low amplitude at high frequencies. This is because, under the low-frequency high-amplitude condition (condition f in Figure 18), the liquid phase in the vessel is rapidly dispersed, which is similar to the vibration parameters of f = 60 Hz and A = 6 mm, as shown in Figure 9. This facilitates the full-field motion of the liquid phase in the vessel and relieves the blockage condition in the vessel, resulting in higher mixing efficiency. This suggests that, to some extent, increasing the amplitude is more beneficial for improving the mixing effect compared to increasing the vibration frequency under the same acceleration.

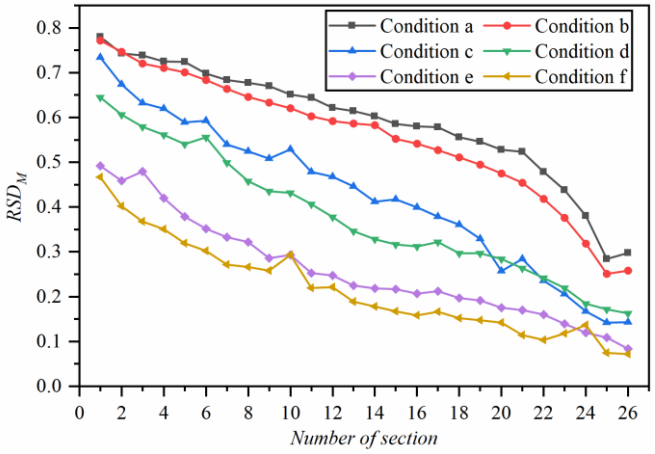

Figure 17. RSD_M of the liquid phase at φ = 90° and a = 588m/s^2, for different A and f over the cross section of the vessel flow channel

The effect of increasing amplitude at constant acceleration on RTD_{avg} and G_{avg} is comparable to that of increasing amplitude at constant frequency, as shown by Figure 18 and 14. As observed in Figure 18, the RTD_{avg} increases with amplitude until it reaches 6 mm (condition e), after which it decreases considerably. G_{avg} increases with amplitude up to A = 4 mm (condition c), beyond which an increase in amplitude causes blockage and a decrease in G_{avg} (condition d). However, when the amplitude is further increased to 7 mm, G_{avg} can be enhanced (condition f). Figure 18 also shows that RSD_M

and RTD_{avg} exhibit a negative correlation, while RSD_M does not show a significant relationship with G_{avg}, which is consistent with the previous findings.

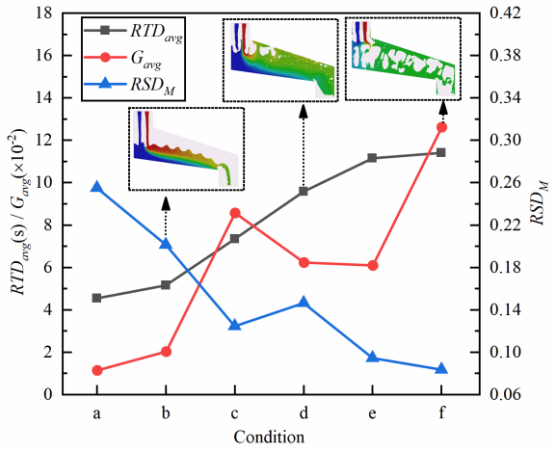

Figure 18. 3D mass concentration fields with a = 588 m/s^2 for different A and f, RTD_{avg}, RSD_M and G_{avg} at Outlet for φ = 90°

4. Data Availability and Reproducibility Statement

The numerical data from Figures 3, 5, 10, 12–18 are tabulated in the Supplementary Material. The simulation model setup case file in Fluent can be obtained in the. zip file as Supplementary Material.

5. Conclusion

This paper presents a numerical simulation model coupled with the VOF and component transport models to investigate the continuous mixing process of high-viscosity fluids in a flow channel under acoustic frequency vibration excitation. The model is experimentally validated and the mixing and transport characteristics are evaluated using RSD_M, RTD_{avg} and G_{avg} indexes. Results show that at lower amplitude acoustic vibration excitation, Faraday waves are generated on the free surface of the liquid, and as the amplitude is gradually increased, the standing waves form disordered jets, deforming the phase interface inside the liquid, and generating a convection field

that effectively promotes mixing. However, increasing the amplitude beyond a certain threshold value causes blockage. If the amplitude is further increased, the high-intensity vibration excitation quickly disperses the liquid in the container, which alleviates the blockage and leads to superior mixing. In this case, the flow field is dominated by shear flow, accompanied by efficient stretching and folding. To achieve efficient mixing at a defined frequency or amplitude, the amplitude and frequency need to reach a certain threshold value.

While changing the amplitude or frequency at a fixed value of the other parameter may lead to a blocking condition, increasing the amplitude at a fixed frequency can alleviate the blockage by promoting full-field dispersion, providing more reflux, and improving mixing without significantly increasing transport time. On the other hand, increasing the frequency at a fixed amplitude not only fails to alleviate the blockage but also hinders reflux generation.

These findings suggest that increasing the amplitude is more effective than increasing the frequency. Moreover, under equal acceleration, low-frequency and high-amplitude conditions are more likely to excite the full-field motion and deformation of the gas-liquid free surface, thereby enhancing reflux and promoting mixing. Overall, this study presents a new approach for continuous mixing of high-viscosity fluids, which has the potential to be applied in various industrial settings.

Acknowledgments. The authors are grateful for the suggestions of the anonymous referees

Funding. This work was supported by the National Natural Science Foundation of China under Grant No.51975226.

Disclosure statement. The authors report there are no competing interests to declare.

References

1. Gao YJ, Ierapetritou M, Muzzio F. Periodic Section Modeling of Convective Continuous Powder Mixing Processes. 10.1002/aic.12563. *Aiche Journal*. Jan 2012;58(1):69-78. doi:10.1002/aic.12563
2. Saeed S, Ein-Mozaffari F, Upreti SR. Using computational fluid dynamics to study the dynamic behavior of the continuous mixing of Herschel-Bulkley fluids. 10.1021/ie800496x. *Industrial & Engineering Chemistry Research*. Oct 1 2008;47(19):7465-7475. doi:10.1021/ie800496x
3. Sui YJ, Lai QX, Nie WF, Tang SS, Wang CS, Bian HG. Wet continuous mixing technique based on full formula of carbon black. *Journal of Applied Polymer Science*. Oct 20 2022;139(40)doi:10.1002/app.52971
4. Lee SH, White JL. Continuous mixing of low viscosity and high viscosity polymer melts in a modular co-rotating twin screw extruder. *International Polymer Processing*. Dec 1997;12(4):316-322. doi:10.3139/217.970316
5. Mashaei P, Hosseinalipour S. Chaotic mixing of high -viscous fluids using a new type of chaotic mixer. *Iranian Chemical Engineering Journal*. 2014;
6. Spencer RS, Wiley RM. The mixing of very viscous liquids. 10.1016/0095-8522(51)90033-5. *Journal of Colloid Science*. 1951;6(2):133-145. doi:10.1016/0095-8522(51)90033-5
7. Dong T, Jiang S, Wu J, Liu H, He Y. Simulation of flow and mixing for highly viscous fluid in a twin screw extruder with a conveying element using parallelized smoothed particle hydrodynamics. *Chemical Engineering Science*. 2020;212:115311. doi:10.1016/j.ces.2019.115311
8. Chen H, Pandey V, Carson S, Maia JM. Enhanced Dispersive Mixing in Twin-Screw Extrusion via Extension-Dominated Static Mixing Elements of Varying Contraction Ratios. 10.3139/217.3857. *International Polymer Processing*. Mar 2020;35(1):37-49. doi:10.3139/217.3857
9. Tran-Minh N, Dong T, Karlsen F. An efficient passive planar micromixer with ellipse-like micropillars for continuous mixing of human blood. 10.1016/j.cmpb.2014.05.007. *Comput Meth Prog Bio*. Oct 2014;117(1):20-9. doi:10.1016/j.cmpb.2014.05.007
10. Oshino S, Nishihama R, Wakamatsu K, et al. Generalization Capability of Mixture Estimation Model for Peristaltic Continuous Mixing Conveyor. 10.1109/ACCESS.2021.3112614. *Ieee Access*. 2021;9:138866-138875. doi:10.1109/Access.2021.3112614
11. Edwards W, Fauve S. Patterns and quasi-patterns in the Faraday experiment. 10.1017/S0022112094003642. *Journal of Fluid Mechanics*. 1994;278:123-148. doi:10.1017/S0022112094003642
12. Kumar K, Tuckerman LS. Parametric instability of the interface between two fluids. 10.1017/S0022112094003812. *Journal of Fluid Mechanics*. 2006;279:49-68. doi:10.1017/s0022112094003812
13. Hashimoto H, Sudo S. Dynamic Behavior of Stratified Fluids in a Rectangular Container Subject to Vertical Vibration. 10.1299/jsme1958.28.1910. *Bulletin of JSME*. 1985;28(243):1910-1917. doi:10.1299/jsme1958.28.1910
14. Ito Y, Komori S. A vibration technique for promoting liquid mixing and reaction in a microchannel. 10.1002/aic.10919. *Aiche Journal*. Sep 2006;52(9):3011-3017. doi:10.1002/aic.10919
15. Vanarase A, Osorio J, Muzzio F, Coguill S, Lucon P. RESONANTACOUSTIC ® MIXING; UNIFORM DISTRIBUTION OF MINOR MATERIALS DURING POWDER MIXING. 2010:

16. Osorio JG, Muzzio FJ. Evaluation of resonant acoustic mixing performance. 10.1016/j.powtec.2015.02.033. *Powder Technology*. Jul 2015;278:46-56. doi:10.1016/j.powtec.2015.02.033
17. Qu Y, Yi W, Guan J. Study on Optimization of Production Efficiency of Acoustic Resonance Mixing for Explosives. *Journal of Ordnance Equipment Engineering*. 2018;39(08):58-62. doi:10.11809/bqzbgcxb2018.08.013
18. Vandenberg A, Wille K. Evaluation of resonance acoustic mixing technology using ultra high performance concrete. 10.1016/j.conbuildmat.2017.12.217. *Construction and Building Materials*. Mar 10 2018;164:716-730. doi:10.1016/j.conbuildmat.2017.12.217
19. Zhang S, Zhan L, Zhang Y, Hou J, Li B. Continuous Flow Resonance Acoustic Mixing Technology: A Novel and Efficient Strategy for Preparation of Nano Energetic Materials. *FirePhysChem*. 2022;3doi:0.1016/j.fpc.2022.08.001
20. Bouarab S, Mokhtari F, Kaddeche S, Henry D, Botton V, Medelfef A. Theoretical and numerical study on high frequency vibrational convection: Influence of the vibration direction on the flow structure. *Physics of Fluids*. Apr 2019;31(4):043605. doi:10.1063/1.5090264
21. Kipriyanov F, Savinykh P. The results of the study of the vibratory conveying machine operating modes. 10.1016/j.trpro.2022.06.067. *Transportation Research Procedia*. 2022;63:721-729. doi:10.1016/j.trpro.2022.06.067.
22. Chen H, Jiang S, Shen Y, Weiwei Z, Li P. A simulation study on conveying characteristics of particles on a vibrating plate with zigzag morphology. IEEE; 2016:468-473.
23. Xiang M, Zhao XY, Zhou HC. Transient dynamic analysis for the submerged gas jet in flowing water. 10.1016/j.euromechflu.2020.09.009. *European Journal of Mechanics B-Fluids*. Jan-Feb 2021;85:351-360. doi:10.1016/j.euromechflu.2020.09.009
24. Bird RB, Armstrong RC, Hassager O, Curtiss CF, Middleman S. Dynamics of Polymeric Liquids, Vols. 1 and 2. 10.1063/1.2994924. *Physics Today*. 1978;31(2):54-57. doi:10.1063/1.2994924
25. Brackbill JU, Kothe DB, Zemach C. A continuum method for modeling surface tension. 10.1016/0021-9991(92)90240-Y. *Journal of Computational Physics*. 1992;100(2):335-354. doi:10.1016/0021-9991(92)90240-y
26. Huang FL, Wang DF, Li ZP, Gao ZM, Derksen JJ. Mixing process of two miscible fluids in a lid-driven cavity. 10.1016/j.cej.2019.01.024. *Chemical Engineering Journal*. Apr 15 2019;362:229-242. doi:10.1016/j.cej.2019.01.024
27. Zhan XB, He Y, Sun ZB, Shen BJ, Li XW. Mixing Characteristics of High-Viscosity Fluids under Forced Vertical Vibration. 10.1002/ceat.201800546. *Chemical Engineering & Technology*. Jul 2020;43(7):1327-1335. doi:10.1002/ceat.201800546
28. Tian S, Barigou M. An improved vibration technique for enhancing temperature uniformity and heat transfer in viscous fluid flow. 10.1016/j.ces.2014.11.029. *Chemical Engineering Science*. Feb 17 2015;123:609-619. doi:10.1016/j.ces.2014.11.029
29. Bekaert B, Grymonpre W, Novikova A, Vervaet C, Vanhoorne V. Impact of blend properties and process variables on the blending performance. 10.1016/j.ijpharm.2021.121421. *International Journal of Pharmaceutics*. Feb 5 2022;613:121421. doi:10.1016/j.ijpharm.2021.121421
30. Guo XF, Fan YB, Luo LG. Residence time distribution on flow characterisation of multichannel systems: Modelling and experimentation. 10.1016/j.expthermflusci.2018.08.016. *Experimental Thermal and Fluid Science*. Dec 2018;99:407-419. doi:10.1016/j.expthermflusci.2018.08.016

31. Yang J, Wang D, Luo Z, Zeng W. Influence of reflux ratio on the anaerobic digestion of pig manure in leach beds coupled with continuous stirred tank reactors. *Waste Manag*. Sep 2019;97(1):115-122. doi:10.1016/j.wasman.2019.08.005
32. Cheng JJ, Manas ZI. Flow Field Characterization in a Banbury Mixer. *International Polymer Processing*. 1990;5(3):178-183. doi:10.3139/217.900178